Controlling the Spontaneous Emission of a Superconducting Transmon Qubit

A. A. Houck,[1] J. A. Schreier,[1] B. R. Johnson,[1] J. M. Chow,[1] Jens Koch,[1] J. M. Gambetta,[2] D. I. Schuster,[1] L. Frunzio,[1] M. H. Devoret,[1] S. M. Girvin,[1] and R. J. Schoelkopf[1]

[1]*Departments of Physics and Applied Physics, Yale University, New Haven, Connecticut 06520, USA*
[2]*Institute for Quantum Computing and Department of Physics and Astronomy, University of Waterloo, Waterloo, Ontario, Canada N2L 3G1*

(Received 31 March 2008; published 21 August 2008)

We present a detailed characterization of coherence in seven transmon qubits in a circuit QED architecture. We find that spontaneous emission rates are strongly influenced by far off-resonant modes of the cavity and can be understood within a semiclassical circuit model. A careful analysis of the spontaneous qubit decay into a microwave transmission-line cavity can accurately predict the qubit lifetimes over 2 orders of magnitude in time and more than an octave in frequency. Coherence times T_1 and T_2^* of more than a microsecond are reproducibly demonstrated.

DOI: 10.1103/PhysRevLett.101.080502 PACS numbers: 03.67.Lx, 42.50.−p, 85.25.−j

Coherence poses the most important challenge for the development of a solid-state quantum computer. As the dephasing time T_2^* can never exceed twice the relaxation time T_1, it is the relaxation time which ultimately sets the limit on qubit coherence. Although T_2^* turned out to be small compared to T_1 in the earliest superconducting qubits [1], steady progress over the past decade has significantly reduced this gap [2–6]. Recently, the transmon, a new type of qubit immune to $1/f$ charge noise, has been shown to be nearly homogeneously broadened ($T_2^* \simeq 2T_1$) [6]. Therefore, understanding relaxation mechanisms is becoming critical to further improvements in both T_1 and T_2^*. Progress in this direction will be based on the accurate modeling of contributions to T_1 and the reliable fabrication of many qubits reaching consistent coherence limits.

One of the main advantages of superconducting qubits is their strong interaction with the wires of an electrical circuit, making their integration with fast control and readout possible and allowing for large, controllable couplings between widely separated qubits [7]. The large coupling also implies a strong interaction between the qubits and their electromagnetic environment, which can lead to a short T_1. However, careful control of the coupling to the environment has been shown to allow prevention of circuit dissipation [8,9]. Relaxation times have been studied in a wide variety of superconducting qubits, created with different fabrication techniques, and measured with a multitude of readout schemes. Typically, values of T_1 vary strongly from sample to sample as they can depend on many factors including materials, fabrication, and the design of both readout and control circuitry. In some instances a separation of these components has been achieved [10–13], but typically it is difficult to understand the limiting factors, and T_1 often varies strongly even among nominally identical qubit samples.

Here, we demonstrate that in a circuit quantum electrodynamics (QED) architecture, where qubits are embedded in a microwave transmission line cavity [3,14], transmon qubits have reproducible and understandable relaxation times. Because of the simple and well-controlled fabrication of the qubit and the surrounding circuitry, involving only two lithography layers and a single cavity for both control and readout, we are able to reliably understand and predict qubit lifetimes. This understanding extends to a wide variety of different qubit and cavity parameters. We find excellent agreement between theory and experiment for seven qubits over 2 orders of magnitude in relaxation time and more than an octave in frequency. The relaxation times are set by either spontaneous emission through the cavity, called the Purcell effect [15], or a shared intrinsic limit consistent with a lossy dielectric. Surprisingly, relaxation times are often limited by electromagnetic modes of the circuit which are far detuned from the qubit frequency. In the circuit QED implementation studied here, the infinite set of cavity harmonics reduces the Purcell protection of the qubit at frequencies above the cavity frequency.

Generally, any discrete-level system coupled to the continuum of modes of the electromagnetic field is subject to radiative decay. By modifying the density of states, the rate of emission can be strongly enhanced [15,16] or suppressed [17–19]. This effect is named after Purcell [15], who first considered this phenomenon in the context of a two-level system coupled to external circuitry. In atomic physics, the same effect is obtained by placing the atom in a cavity, which affords protection from spontaneous emission. Traditionally, one considers the scenario where all but the fundamental mode of the cavity are far detuned from the atomic transition frequency so that all higher modes can be neglected. Then, a single-mode approximation can be used and the Purcell rate for dispersive decay is given by $\gamma_\kappa = (g/\Delta)^2\kappa$, where g denotes the coupling between qubit and cavity mode, Δ their mutual detuning, and κ the average photon loss rate. However, this approximation

is inadequate for solid-state systems with strong coupling and a treatment going beyond a single mode is necessary.

We can arrive at the same physics using a circuit model, which can subsequently be extended to include higher harmonics. For concreteness, we consider the case of a qubit capacitively coupled to an arbitrary environment with impedance $Z_0(\omega)$; see Fig. 1(a). This circuit may be reduced to a qubit coupled to an effective dissipative element; see Fig. 1(b). Specifically, replacing the coupling capacitor C_g and the environment impedance Z_0 by an effective resistor $R = 1/\mathrm{Re}[Y(\omega)]$, one finds [8,9] that the T_1 is given by RC, where C is the qubit capacitance. Choosing a purely resistive environment, $Z_0 = 50\ \Omega$, yields a decay rate $\gamma \simeq \omega^2 Z_0 C_g^2/C$. If instead we couple to a parallel LRC resonator, the calculated radiation rate can be reduced to that of the atomic case, $\gamma_\kappa = (g/\Delta)^2\kappa$, thus reproducing the Purcell effect with the single-mode approximation.

The qualitative features of the single-mode Purcell model are apparent in measurements of T_1, shown for 3 qubits in Fig. 2, measured with a dispersive readout by varying a delay time between qubit excitation and measurement [6,20]. Near the cavity resonance at 5.2 GHz, spontaneous emission is Purcell-enhanced and T_1 is short. Away from resonance, the cavity protects the qubit from decay and the relaxation time is substantially longer than expected for decay into a continuum. However, at detunings above the cavity frequency, the measured T_1 deviates significantly from the single-mode Purcell prediction. This deviation can be directly attributed to the breakdown of the single-mode approximation.

The breakdown of the single-mode model arises from the striking impact of higher harmonics on relaxation times. In fact, the coupling g_n to the nth mode of the cavity increases with mode number, $g_n = g_0\sqrt{n+1}$. In addition, the input and output capacitors act as frequency-dependent mirrors, so that the decay rate of the nth harmonic, $\kappa_n = (n+1)^2\kappa$, is larger than that of the fundamental. As a result, higher modes significantly contribute to the qubit decay rate, and the simple single-mode quantum model turns out to be inadequate for understanding the T_1 of the system. The naive attempt to treat the fundamental and harmonics in terms of a multimode Jaynes-Cummings Hamiltonian faces problems with divergences. Work on developing a consistent quantum model is currently under way [21].

Here, we follow the alternative route of calculating T_1 by extending the circuit model to include the full underlying circuit, and show that this accurately reproduces the measured T_1. The relationship between the classical admittance $Y(\omega)$ of a circuit and its dissipation has long been known [8,9], providing a practical means of understanding relaxation rates [12]. The full calculation includes a transmission line cavity rather than a simple LRC resonator; see Fig. 1(c). The results from this are shown in Fig. 2, and reveal two striking differences as compared to the single-

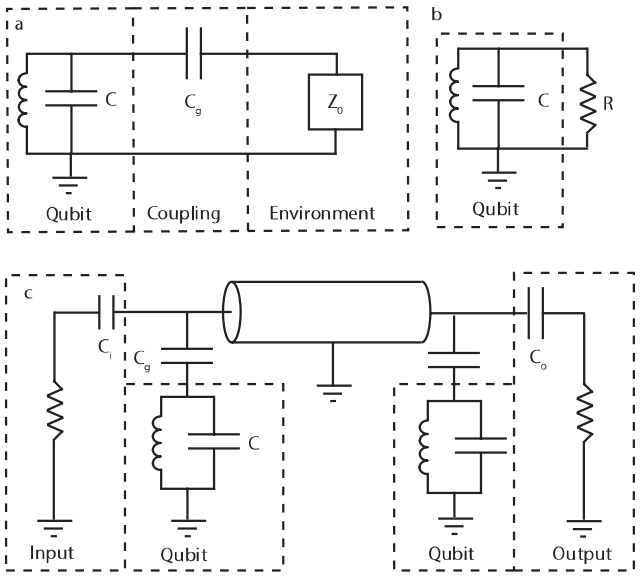

FIG. 1. Circuit model of qubit relaxation. (a) Generalized model for a qubit coupled to an environment. (b) Reduced model of dissipation. The coupling capacitor and environment impedance are replaced by an effective resistance $R = 1/\mathrm{Re}[Y(\omega)]$, where $Y(\omega)$ is the admittance of the rest of the circuit seen by the qubit. The T_1 for the qubit is RC, where C is the qubit capacitance. (c) Full circuit diagram. Qubits are capacitively coupled to either end of a transmission-line cavity. Both the input and output of the cavity are connected to a 50 Ω environment. The cavity is asymmetric in the sense that the input capacitance is smaller than the output capacitance.

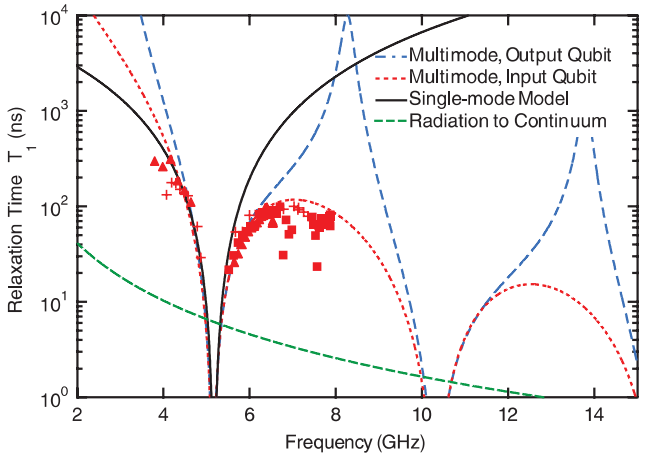

FIG. 2 (color). Comparison of multimode and single-mode models of relaxation. Spontaneous emission lifetimes into a single-mode cavity are symmetric about the cavity frequency, while within the multimode model lifetimes below the cavity are substantially longer than above. The measured T_1 for three similar qubits deviates substantially from the single-mode prediction, but agrees well with the multimode model. The expected decay time for radiation into a continuum is shown for comparison.

mode model. First, there is a strong asymmetry between relaxation times for qubit frequencies above (positive detuning) and below (negative detuning) the fundamental cavity frequency. While the single-mode model predicts identical relaxation times for corresponding positive and negative detunings, T_1 can be 2 orders of magnitude shorter for positive detunings than for negative detunings in the multimode model. Second, the multimode model shows a surprising dependence of T_1 on the qubit position in the cavity. While qubits located at opposite ends of the cavity have the same T_1 within the single-mode model, the multimode model correctly captures the asymmetry induced by the differing input and output coupling capacitors and leads to vastly different T_1. The multimode model accurately resolves the discrepancy between the experimental data and the single-mode model; see Fig. 2.

The predictive power of the multimode model extends to all of our transmon qubits. Here, we present T_1 measurements on a representative selection of seven qubits. The qubits were fabricated on both oxidized high-resistivity silicon and sapphire substrates, and coupled to microwave cavities with various decay rates and resonant frequencies. Table I provides parameters for each of the seven qubits. Qubits are fabricated via electron beam lithography and a double-angle evaporation process (25 and 80 nm layers of aluminum), while cavities are fabricated by optical lithography with either lifted-off Al or dry-etched Nb on a Si or sapphire substrate [22].

Predictions from the multimode model are in excellent agreement with observed qubit lifetimes (see Fig. 3), up to a $Q = 70\,000$ for qubits on sapphire. The agreement is valid over more than 2 orders of magnitude in qubit lifetime and more than an octave of frequency variation. We emphasize that the multimode model does not correspond to a fit to the data, but rather constitutes a prediction based on the independently measured cavity parameters ω_r and κ, and the coupling g.

In the qubits on silicon, coherence times of no more than 100 ns are observed above the cavity resonance, far below predictions from the single-mode model, but consistent with the multimode model. Initially, this caused concern for the transmon qubit: it appeared as if the transmon solved the $1/f$-noise dephasing problem for charge qubits, but introduced a new relaxation problem [23–25]. However, with the multimode model of relaxation, it is now clear that the 100 ns limit originated from the surprisingly large spontaneous emission rate due to higher cavity modes. By working at negative detunings instead, it is possible to achieve longer relaxation times.

All qubits on sapphire substrates reach a shared intrinsic limit of $Q = 70\,000$ when not otherwise Purcell limited, resulting in T_1 up to 4 μs. The constant-Q frequency dependence of the intrinsic limit ($T_1 \propto 1/\omega$) is suggestive of dielectric loss as the likely culprit. The observed loss tangent, $\tan\delta \sim 10^{-5}$, is worse than loss tangents of $\sim 10^{-9}$ in bulk sapphire [26]. This increased loss may be attributed to two-level systems at the surface [27] as the electric fields of the transmon are localized near the surface of the sapphire substrate. The overall reproducibility of the intrinsic limit gives hope that future experiments may isolate its cause and reveal a solution. It is instructive to reexpress the relaxation times in terms of a parasitic resistance; see Fig. 3. Note that here a T_1 of a microsecond roughly corresponds to a resistance of 20 MΩ. To build more complex circuits with still longer T_1, all dissipation due to parasitic couplings must be at the GΩ level.

Transmon qubits benefit greatly from the increased relaxation times, as they are insensitive to $1/f$-charge noise,

TABLE I. Qubit parameters. Sample 1 is a single-qubit sample, all others are two-qubit samples. The Resonator column indicates material and substrate for the cavity. The Pos. column indicates the position of the qubit at the input or output end of the cavity.

ID	Resonator	$\omega_r/2\pi$ (GHz)	$\kappa/2\pi$ (MHz)	$g/2\pi$ (MHz)	Pos.
1	Al on Si	5.17	44	107	In
2L	Al on Si	5.19	33	105	In
2R	Al on Si	5.19	33	105	Out
3L	Nb on sapphire	6.69	40	166	In
3R	Nb on sapphire	6.69	40	50	Out
4L	Nb on sapphire	6.905	0.7	150	In
4R	Nb on sapphire	6.905	0.7	55	Out

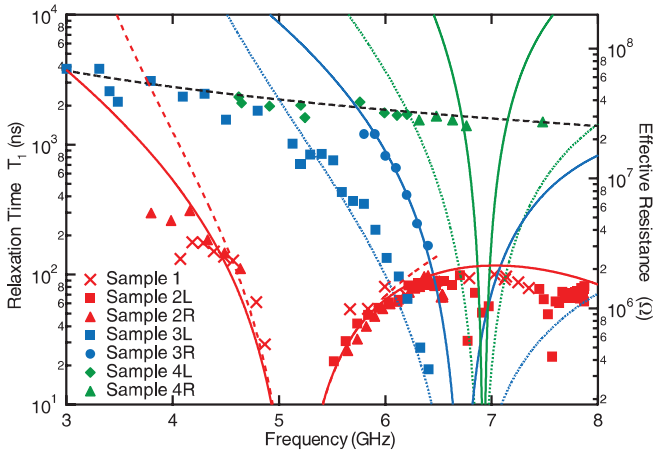

FIG. 3 (color). Relaxation times for seven superconducting qubits. Predictions for qubit lifetime based on the circuit model (colored lines) agree well with observed relaxation times (points). Solid lines represent predictions for input side (L) qubits, while dashed lines correspond to output side (R) qubits. All sapphire qubits (blue and green) reach the same common intrinsic limits (black line), with lifetimes limited to a constant $Q \sim 70\,000$. Some deviation is seen in the lowest frequency silicon qubits, though it is unclear if this is an intrinsic limit. Qubit lifetimes are accurately predicted over a wide range of frequencies and more than 2 orders of magnitude in time.

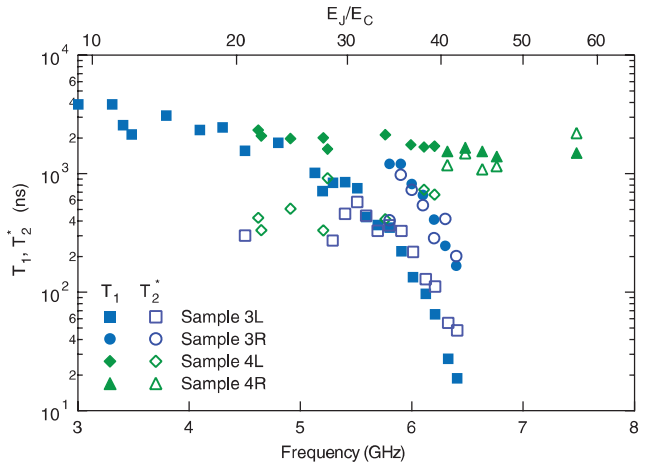

FIG. 4 (color). Dephasing times for four sapphire qubits. Measured dephasing times for each of the four sapphire qubits are nearly homogeneously broadened, with T_2^* (open symbols) similar to T_1 (closed symbols) over a wide range of frequencies, even away from the flux sweet spot (probed only by sample 4R). Charge noise is suppressed exponentially in the ratio of Josephson to charging energies E_J/E_C (top axis), tuned along with qubit frequency (bottom axis) by changing an applied magnetic field. For small E_J/E_C charge noise dephasing is relevant and causes short T_2^*.

the primary source of dephasing in other charge qubits. As a result, coherence is limited primarily by energy relaxation and transmons are nearly homogeneously broadened ($T_2^* \simeq 2T_1$). Improvements in T_1 thus translate directly into improvements in dephasing times T_2^*. This is demonstrated in Fig. 4, showing a comparison of relaxation and dephasing times. Here, T_2^* is measured in a pulsed Ramsey experiment and without echo, fitting to an exponential or a Gaussian depending on the type of broadening [6]. The gain in coherence time is most striking in samples with a higher-frequency cavity, $\omega_r/(2\pi) \sim 7$ GHz, where it is easier to operate at negative detunings and attain long T_1. In all these samples, we observe consistently long dephasing times of nearly a microsecond, with the largest T_2^* exceeding 2 μs without echo.

There are two main effects determining the observed dependence of T_2^* on the qubit frequency. First, away from the maximum frequency for each qubit, i.e., the flux sweet spot [2], the sensitivity to flux noise increases. This can cause additional inhomogeneous broadening. Despite this, T_2^* remains close to 2 μs, even away from the flux sweet spot. Second, tuning the qubit frequency via E_J directly affects the ratio of Josephson to charging energy, E_J/E_C, which dictates the sensitivity to charge noise and is discussed quantitatively in Ref. [6]. At qubit frequencies below 5 GHz, the qubits regain the charge sensitivity of the Cooper pair box, thus explaining the strong drop in dephasing times seen in Fig. 4.

The concise understanding of spontaneous emission lifetimes in our system and the reproducibility of intrinsic lifetimes open up vistas for a systematic exploration of limits on coherence. As we have shown here, even far off-resonant modes of a cavity can have a dramatic impact on qubit lifetimes. With careful design, it should be possible not only to avoid additional accidental resonances, but to utilize appropriate models of relaxation to build filters to minimize dissipation. This is not only important for superconducting qubits, but, ultimately, will be relevant for other strongly coupled quantum systems such as quantum-dot based cavity QED [28].

This work was supported in part by Yale University (A. A. H., J. K.), by CNR-Istituto di Cibernetica (L. F.), by LPS/NSA under ARO Contract No. W911NF-05-1-0365, and the NSF under Grants No. DMR-0653377 and No. DMR-0603369.

[1] Y. Nakamura, Y. A. Pashkin, and J. S. Tsai, Nature (London) **398**, 786 (1999).
[2] D. Vion *et al.*, Science **296**, 886 (2002).
[3] A. Wallraff *et al.*, Nature (London) **431**, 162 (2004).
[4] P. Bertet *et al.*, Phys. Rev. Lett. **95**, 257002 (2005).
[5] M. Steffen *et al.*, Phys. Rev. Lett. **97**, 050502 (2006).
[6] J. A. Schreier *et al.*, Phys. Rev. B **77**, 180502(R) (2008).
[7] R. J. Schoelkopf and S. M. Girvin, Nature (London) **451**, 664 (2008).
[8] D. Esteve, M. H. Devoret, and J. M. Martinis, Phys. Rev. B **34**, 158 (1986).
[9] M. H. Devoret *et al.*, in *Exploring the Quantum/Classical Frontier*, edited by J. R. Friedman and S. Han (Nova Science, New York, 2003).
[10] P. Bertet *et al.*, arXiv:cond-mat/0412485.
[11] J. M. Martinis *et al.*, Phys. Rev. Lett. **95**, 210503 (2005).
[12] M. Neeley *et al.*, Phys. Rev. B **77**, 180508(R) (2008).
[13] O. Astafiev *et al.*, Phys. Rev. B **69**, 180507 (2004).
[14] A. Blais *et al.*, Phys. Rev. A **69**, 062320 (2004).
[15] E. M. Purcell, Phys. Rev. **69**, 681 (1946).
[16] P. Goy *et al.*, Phys. Rev. Lett. **50**, 1903 (1983).
[17] D. Kleppner, Phys. Rev. Lett. **47**, 233 (1981).
[18] R. G. Hulet, E. S. Hilfer, and D. Kleppner, Phys. Rev. Lett. **55**, 2137 (1985).
[19] W. Jhe *et al.*, Phys. Rev. Lett. **58**, 666 (1987).
[20] A. Wallraff *et al.*, Phys. Rev. Lett. **95**, 060501 (2005).
[21] J. M. G. Gambetta *et al.* (to be published).
[22] L. Frunzio *et al.*, IEEE Trans. Appl. Supercond. **15**, 860 (2005).
[23] D. I. Schuster *et al.*, Nature (London) **445**, 515 (2007).
[24] J. Majer *et al.*, Nature (London) **449**, 443 (2007).
[25] A. A. Houck *et al.*, Nature (London) **449**, 328 (2007).
[26] V. B. Braginsky and V. I. Panov, IEEE Trans. Magn. **15**, 30 (1979); V. B. Braginsky, V. S. Ilchenko, and K. S. Bagdassarov, Phys. Lett. A **120**, 300 (1987).
[27] J. Gao *et al.*, Appl. Phys. Lett. **92**, 152505 (2008).
[28] J. P. Reithmaier *et al.*, Nature (London) **432**, 197 (2004); T. Yoshie *et al.*, Nature (London) **432**, 200 (2004).